Evaluating the Impact of Yoga Practices to Improve Chronic Venous Insufficiency Symptoms: A Classification by Gaussian Process

Feng Yun Gou
Inner Mongolia University of Technology Hohhot, Inner Mongolia, 010051, China

***Abstract*—Chronic Venous Insufficiency (CVI) is a widespread condition marked by diverse venous system irregularities stemming from occlusion and varicosities. Factors like family history and lifestyle choices amplify CVI's economic consequences, emphasizing the need for proactive measures. The sedentary lifestyle of many individuals can contribute to various diseases, including CVI. Yoga is now endorsed as a multifaceted exercise to alleviate CVI symptoms, offering a holistic approach and complementary therapy for diverse medical conditions. This study developed a method for evaluating and classifying symptoms associated with varicose veins, utilizing the Venous Clinical Score (VCSS) data. A specific emphasis was placed on investigating the impact of yoga on these symptoms, and a comprehensive performance assessment was conducted based on data obtained from a cohort of 100 patients. This paper achieves optimal performance by employing the Gaussian Process Classifier (GPC) along with two optimizers, namely the Crystal Structure Algorithm (CSA) and the Fire Hawk Optimizer (FHO). The results indicate that in predicting VCSS-Pre (reflecting symptoms before engaging in yoga exercises), the GPFH exhibited superior performance with an F1-score of 0.872, surpassing the GPCS, which attained an F1-score of 0.861 by almost 1.26%. Additionally, the prediction for VCSS-1, reflecting symptoms after one month of yoga practices, revealed the GPFH outperforming the GPCS with respective F1-score values of 0.910 and 0.901.**

Keywords*—*Chronic venous insufficiency; yoga; Gaussian Process Classifier; Crystal Structure Algorithm; Fire Hawk Optimizer

I. INTRODUCTION

Prolonged sitting, prevalent in contemporary office environments that have shifted from active to passive, poses a risk for cardio-metabolic diseases, type 2 diabetes, obesity, coronary artery disease, musculoskeletal conditions, certain cancers, and early death [1], [2]. Sedentary behavior, considered by an energy expenditure of $\leq 1.5\ METs$ while sitting or reclining, is a substantial issue in modern workplaces [3]. Extended periods of sitting have been correlated with elevated risks of obesity and diabetes, with studies indicating a 5% rise in obesity risk and a 7% increase in diabetes risk for every two-hour increase in sitting time [4]. Moreover, prolonged sitting is linked to a heightened possibility of musculoskeletal disorders, particularly low back pain [5]. Other research has demonstrated that occupations requiring significant periods of sedentary behavior are associated with an increased risk of developing certain types of cancers, such as endometrial, prostate, and colorectal cancer [6], [7].

Inactive sitting behavior is closely associated with the risk of cardiovascular disease (CVD), irrespective of one's level of physical activity. This association arises from the impact of sedentary behavior on crucial inflammatory, hemodynamic, and metabolic processes, leading to compromised arterial health. Consequently, these vascular issues directly and indirectly contribute to the development of cardiovascular disease [8], [9]. Some studies have revealed a noteworthy correlation between the duration of individuals' sitting hours in the workplace and the incidence of Chronic Venous Insufficiency (CVI). This association underscores a substantial escalation in the risk of contracting such conditions [10], [11], [12].

CVI is widespread in both developing and developed nations [13]. As outlined in the American Venous Forum's consensus statement, CVI involves various morphological and practical irregularities in the venous system, from telangiectasias to venous ulcers [14]. The recognition of CVI lacks a specific date, but the historical understanding of venous insufficiency can be traced to ancient times when Egyptians, Greeks, and Romans described similar symptoms. In the 17th century, William Harvey, an English physician, significantly advanced the understanding of the circulatory system, though the term "Chronic Venous Insufficiency" is a more recent medical terminology. The precise historical origin of this term is unclear, yet the evolving comprehension and management of venous insufficiency have shaped current diagnostic criteria and treatment approaches [15], [16].

CVI refers to pathological changes in the lower extremities' tissues resulting from anomalies in venous blood flow. These glitches encompass popliteal or iliofemoral vein occlusion, incompetence, and varicosities, mainly in the greater saphenous system associated with valvular leakage or abnormal arteriovenous communications. In some cases, chronic venous insufficiency can arise from large acquired arteriovenous fistulae, certain congenital anomalies, or tumors of the blood vessels [17], [18]. CVI risk factors encompass factors such as family history, aging, long-standing, obesity, an inactive routine, smoking, lower extremity trauma, previous venous thrombosis, the existence of an arteriovenous shunt, high estrogen states, and pregnancy [19], [20], [21]. The economic consequences of CVI are evident through increased health care costs, potential productivity loss due to symptoms such as leg pain and swelling, and the potential threat of disability leading

to unemployment. These challenges have a double effect on individuals and society in general. Implementing effective preventive measures, timely interventions, and creating supportive facilities in the workplace appear as central strategies for reducing the economic burden associated with CVI [22], [23].

Diagnosing CVI relies on a comprehensive assessment encompassing medical history, observed signs and symptoms, and diagnostic tests. A crucial tool for quantifying disease severity is the Venous Severity Scoring system, introduced in 2000 and refined in 2010 [24]. This system comprises three components: The Venous Clinical Severity Score (VCSS), which evaluates clinical symptoms; The Venous Segmental Disease Score (VSDS), which focuses on segment-specific aspects; and the Venous Disability Score (VDS), which provides insights into the functional impact of CVI. These scoring components collectively enhance the accuracy and thoroughness of clinical evaluations for individuals with CVI [25], [26]. Physicians use the VCSS to evaluate the impact of venous disease on a patient's clinical condition and to make informed decisions about appropriate treatment strategies [27].

Presently, yoga is recommended as one of the activities to alleviate symptoms associated with CVI [28]. Yoga, originating in ancient India, is a holistic practice encompassing physical, mental, and spiritual disciplines. It combines physical postures, breath control, meditation, and ethical principles to promote well-being, harmony, flexibility, strength, stress reduction, and mental clarity [29], [30]. Yoga is increasingly integrated into medical care as a complementary therapy, offering benefits for chronic pain, mental health issues, cardiovascular health, cancer care, respiratory conditions, and rehabilitation.

II. Objective

Utilizing a machine learning (ML) approach, this article delves into the effectiveness of yoga exercises in alleviating symptoms among individuals with chronic venous insufficiency. ML, a subset of artificial intelligence (AI), entails creating algorithms and statistical models that empower computers to execute tasks without explicit programming. It constitutes a field of study wherein systems acquire knowledge and enhance performance through experience, enabling pattern recognition, predictions, and adaptation to new data. These algorithms utilize training data to identify inherent patterns, enabling them to make decisions or predictions without explicit programming for each task. The exploration includes predicting and categorizing these symptoms into distinct classifications using the Gaussian Process Classifier (GPC). For the ultimate optimization, the article incorporates two optimizers, namely, the Crystal Structure Algorithm (CSA) and the Fire Hawk Optimizer (FHO), to achieve optimal performance.

III. Methodology and Modeling Approach

A. Gaussian Process Classifier (GPC)

The Gaussian Process (GP) classifier, grounded in Bayesian theory, operates by establishing a Gaussian prior distribution over the estimated function, represented as $p(x) = w^T x + b$. This initial distribution forms the basis for the probabilistic estimation process, and the classifier further incorporates a sigmoid function to construct a probabilistic estimator as outlined in Eq. (1):

$$p(y = 1|x) = sigmoid(f(x)) \tag{1}$$

Determining the distribution of the latent variable y for a test sample involves two key steps. Firstly, it is computed by leveraging the posterior over the latent variables, denoted as $p(f|X, y)$. Following this, the second step entails calculating a posterior using Eq. (2), which builds upon the outcomes from the initial step. This sophisticated method enables the probabilistic estimation of the latent variable y, providing nuanced insights and accurate predictions.

$$p(y = 1|X, y, x) \tag{2}$$

X and Y denote the training samples, with x representing the test sample. While conducting this inference is generally a complex task, there are existing approximations that tend towards an optimal solution with larger datasets. Furthermore, kernel versions of this process offer a more straightforward approach [31].

B. Fire Hawk Optimizer (FHO)

The FHO algorithm replicates the foraging patterns of Fire Hawks, involving the initiation and expansion of fires to capture prey. It commences by generating a set of potential solutions (X) inspired by the position vectors of fire hawks and their prey. The initial positioning of these vectors within the search space is determined randomly, imitating the initial locations of fire hawks and prey, laying the foundation for subsequent optimization stages [32].

$$x = \begin{bmatrix} x_1 \\ x_2 \\ \vdots \\ x_i \\ \vdots \\ x_n \end{bmatrix} = \begin{bmatrix} x_1^1 & x_1^2 & \cdots & x_1^j & \cdots & x_1^d \\ x_2^1 & x_2^2 & \cdots & x_2^j & \cdots & x_2^d \\ \vdots & \vdots & \vdots & \vdots & \vdots & \vdots \\ x_i^1 & x_i^2 & \dots & x_i^j & \dots & x_i^d \\ \vdots & \vdots & \vdots & \vdots & \vdots & \vdots \\ x_N^1 & x_N^2 & \cdots & x_N^j & \dots & x_N^d \end{bmatrix}, \begin{cases} i = 1,2,3,\dots,N. \\ j = 1,2,3,\dots,d. \end{cases} \tag{3}$$

$$x_i^j(0) = x_{i,min}^j + rand.\left(x_{i,max}^j - x_{i,min}^j\right), \begin{cases} i = 1,2,3,\dots,N. \\ j = 1,2,3,\dots,d. \end{cases} \tag{4}$$

X_i represents solution candidates, d is the problem dimension, N is the total number of candidates, x_i^j is a decision variable, $x_i^j(0)$ is the initial position, $x_{i,max}^j$, $x_{i,min}^j$ are variable bounds, and $rand$ is a random number (0, 1). The goal is to identify Fire Hawks in the search space based on higher objective function values. Selected Fire Hawks spread flames around prey, aiding hunting. The primary fire, initially used by Fire Hawks, is assumed to represent the best global solution.

$$PR = \begin{bmatrix} PR_1 \\ PR_2 \\ \vdots \\ PR_i \\ \vdots \\ PR_m \end{bmatrix}, i = 1,2,3,\dots,m \tag{5}$$

$$FH = \begin{bmatrix} FH_1 \\ FH_2 \\ \vdots \\ FH_i \\ \vdots \\ FH_n \end{bmatrix}, i = 1,2,3, \dots, n \quad (6)$$

PR_i signifies the i_{th} fire hawk, and FH_i denotes the i_{th} prey, where *n* is the total number of prey. The subsequent step involves calculating the distance between Fire Hawks and their prey, with D_l^k expressed by the following equation:

$$D_l^k = \sqrt{(x_2 - x_1)^2 + (y_2 - y_1)^2}, \begin{cases} k = 1,2,3, \dots, n. \\ l = 1,2,3, \dots, m. \end{cases} \quad (7)$$

The exploration space's total count of prey and fire hawks is denoted by n and m, respectively. The cumulative distance among the i_{th} Fire Hawk (FH) and prey, represented by D_l^k, is determined by the coordinates (x_1, y_1) for FH and (x_2, y_2) for prey. The birds establish territories by classifying the nearest prey and calculating total distances. Gathering hot coals from the main fire to ignite specific spots and engaging in behaviors such as using burning sticks from other territories serve as position updates in the $FHO's$ primary search loop.

$$FH_i^{new} = FH_i + (r_1 \times GB - r_2 \times FH_{near}), i = 1,2,3, \dots, n \quad (8)$$

The primary fire, denoted as GB, signifies the global best solution in the search space. FH_i^{new} represents the new location vector of the i_{th} FH, while r_1 and r_2 are uniformly distributed random numbers in the range $(0, 1)$ representing movements towards the primary fire and other Fire Hawks' territories. FH_{near} designates one of the FH within the exploration space. The algorithm's next stage involves prey movements during fires and guiding position updates. An equation is employed for these actions during place updates to incorporate the importance of territory in animal behavior.

$$PR_s^{new} = PR_s + (r_3 \times FH_i - r_4 \times SP_i), \begin{cases} i = 1,2,3, \dots, n \\ s = 1,2,3, \dots, r \end{cases} \quad (9)$$

The new position vector of the S_{th} prey (PR_s), surrounded by the i_{th} Fire Hawk (FH_i), is represented as PR_s^{new}. SP_i signifies a safe place under the i_{th} Fire Hawk territory. To monitor prey movements toward Fire Hawks and their retreat to safe zones, r_3 and r_4 are uniformly distributed random integers from 0 to 1. Prey may venture into other FH territories or approach those trapped by flames. FH might seek safer areas beyond their territory. The provided equations accommodate these actions in position updates.

$$PR_i^{new} = PR_i + (r_5 \times FH_{Alter} - r_6 \times SP), \begin{cases} i = 1,2,3, \dots, n \\ s = 1,2,3, \dots, r \end{cases} \quad (10)$$

The updated position vector of the i_{th} prey (PR_i), positioned between the i_{th} Fire Hawk (FH_i), is denoted as PR_i^{new}. SP represents a secure area beyond the i_{th} FH territory. FH_{Alter} signifies one of the FH in the search space. The movements of prey toward other FH and the secure region beyond their territories are determined by the uniformly distributed values of r_5 and r_6 in the range (0,1).

The mathematical expression for SP_i and SP is derived with the acknowledgment that, in the natural environment, a secure location is where most animals gather for protection during threats.

$$SP_i = \frac{\sum_{s=1}^{r} PR_s}{r}, \begin{cases} i = 1,2,3, \dots, n \\ s = 1,2,3, \dots, r \end{cases} \quad (11)$$

$$SP = \frac{\sum_{q=1}^{m} PR_q}{m}, q = 1,2,3, \dots, m \quad (12)$$

PR_s represents the prey positioned around the S_{th} fire hawk (FH_i), while PR_q denotes the q_{th} prey within the search space.

C. Crystal Structure Algorithm (CSA)

Solid minerals, comprised of atoms and particles arranged in a crystalline form known as crystals, derive their Grecian meaning from the concept of solidification by cold. Interior particles were initially discovered in 1619 by Kepler, 1665 Hooke, and 1690 Hogens [33]. Crystals display a repeating pattern of atoms in defined spaces, forming a lattice that not only dictates the crystal's shape but also inspires geometric figures derived from infinite natural shapes. The discontinuous crystal structure is crafted by considering an infinite lattice, with each lattice point linked to its position through a vector [34]:

$$r = \sum m_i \, d_i \quad (13)$$

The variables in the model are defined as follows: m_i is an integer, d_i represents the shortest vector along the central crystallographic directions, and i corresponds to the number of crystal corners. The mathematical model of CryStAl is then introduced in this section, incorporating fundamental crystal concepts with notable modifications. The crystal number is initialized as a random number in this model.

$$Cr = \begin{bmatrix} Cr_1 \\ Cr_2 \\ \vdots \\ Cr_i \\ \vdots \\ Cr_n \end{bmatrix} = \begin{bmatrix} x_1^1 & x_1^2 & \dots & x_1^j & \dots & x_1^d \\ x_2^1 & x_2^2 & \dots & x_2^j & \dots & x_2^d \\ \vdots & \vdots & \vdots & \vdots & \vdots & \vdots \\ x_i^1 & x_i^2 & \dots & x_i^j & \dots & x_i^d \\ \vdots & \vdots & \vdots & \vdots & \vdots & \vdots \\ x_n^1 & x_n^2 & \dots & x_n^j & \dots & x_n^d \end{bmatrix}, \begin{cases} i = 1,2,3, \dots, n \\ j = 1,2,3, \dots, j \end{cases} \quad (14)$$

$$x_i^j(0) = x_{i,min}^j + \xi \left(x_{i,max}^j - x_{i,min}^j\right), \begin{cases} i = 1,2,3, \dots, n \\ j = 1,2,3, \dots, d \end{cases} \quad (15)$$

In this model, n and d denote the number of crystals and the problem's dimension, respectively. The variables $x_i^j(0)$, $x_{i,max}^j$ and $x_{i,min}^j$ determine the initial positions and permissible values for each decision variable of candidate solutions, while ξ is a random number within [0,1] . Following crystallography principles, primary crystals Cr_m are corner crystals randomly chosen, and the main crystal is selected in each step, excluding the current one. F_c represents the mean merit of randomly chosen crystals and Cr_b is the best-arranged crystal. Based on fundamental lattice cross-section standards, four types of

improvement processes are specified for upgrading candidate arrangements in this crystal model.

Cubicles;

Simple:

$$Cr_n = Cr_o + aCr_m \quad (16)$$

With the finest crystals:

$$Cr_n = Cr_o + a_1 Cr_m + a_2 Cr_b \quad (17)$$

With the mediocre crystals:

$$Cr_n = Cr_o + a_1 Cr_m + a_2 f_c \quad (18)$$

With the finest and mediocre crystals:

$$Cr_n = Cr_o + a_1 Cr_m + a_2 Cr_b + a_3 F_c \quad (19)$$

The set of four equations illustrates the transition between new and old positions, denoted as Cr_n and Cr_o, respectively, incorporating fortuitous numbers a, a_1, a_2 and a_3. The algorithm employs exploration and extraction features, calculated using Eq. (16) to Eq. (19). The optimization process concludes upon reaching the maximum iteration, adhering to a predefined termination criterion with a fixed number of repetitions. A mathematical flag is utilized for solution variables x_i^j, indicating the exterior of factors range and setting a boundary change order.

The CSA pseudo
− code is shown below: Procedure Crystal Structure Algorith
randomly create values for primary positions (x_i^j) of prima
Estimate fitness values for each crystal
while ($t <$ maximum number of iterations)
for i = 1: number of initial crystals
Create $\boldsymbol{Cr_m}$
Create new crystals by Eq. (16)
Create $\boldsymbol{Cr_b}$
Create new crystals by Eq. (17)
Create $\boldsymbol{F_c}$
Create new crystals by Eq. (18)
Create new crystals by Eq. (19)
if new crystals violate boundary conditions
Control the position constraints for new crystals and amend
end if
Evaluate the fitness values for new crystals
Update Global Best (GB) if a better solution is found
end for
$t = t + 1$
end while
Return GB
End procedure

IV. MATERIAL

A. Data Description and Analysis

Data mining, acknowledged as a crucial element in the Knowledge Discovery from Databases (KDD) process [35], is progressively gaining significance within the healthcare system. It plays a vital role in precisely predicting medical conditions by automating the extraction of knowledge from extensive datasets [36] and employing a spectrum of techniques, including statistical analysis, machine learning, and database methodologies, to facilitate informed decision-making [37].

The dataset provides an extensive and diverse collection of variables, each with the potential to influence the symptoms associated with varicose veins. This well-rounded dataset includes key variables such as Body Mass Index (BMI), Systolic Blood Pressure Type A (SBPA), Systolic Blood Pressure Type B (SBPB), Ankle-Brachial Pressure Index (ABPI), Diabetes Blood Pressure Type A (DBPA), Diabetes Blood Pressure Type B (DBPB), Pulse Rate (PR), Chronic Fatigue Syndrome (CFS), Hyperhomocysteinemia (HCY), Calf Circumference (CALF-CIR), the Chronic Venous Insufficiency Questionnaire (CVIQ), and the Chalder Fatigue Scale (CFS). In addition to these primary variables, the dataset includes two supplementary variables: VCSS-Pre, which represents symptoms observed before the initiation of yoga practices, and VCSS-1, which captures symptoms observed after one month of participation in yoga sessions. These variables provide a unique opportunity to analyze the potential impact of yoga on varicose vein symptoms over time. To facilitate analysis, the dataset has been categorized into four distinct groups based on the severity of the condition: Absent condition (0-5), Mild (6-10), Moderate (11-20), and Severe (21-30). This classification allows for a more structured examination of the relationship between the various factors and the severity of varicose vein symptoms, offering insights that can inform treatment approaches and patient care strategies.

In this research, Fig. 1 illustrates a correlation matrix that provides a detailed and comprehensive view of the intricate interrelationships among the investigated input and output variables. The matrix reveals how the input data not only significantly influences the output but also affects the relationships between other input variables. For example, the Diabetes Blood Pressure indicators, specifically DBPA (Diabetes Blood Pressure Type A) and DBPB (Diabetes Blood Pressure Type B), show a pronounced effect on both SBPA (Systolic Blood Pressure Type A) and SBPB (Systolic Blood Pressure Type B). This highlights the critical role that blood pressure variations, influenced by diabetes, play in shaping systolic blood pressure outcomes. Additionally, the correlation matrix underscores the significant impact of the Chalder Fatigue Scale's physical and mental components (CFS PHY-Pre and CFS MEN-Pre) on the overall CFS-Pre score. These findings suggest that fatigue, as captured by the Chalder scale, is a crucial predictor of overall chronic fatigue syndrome (CFS) severity. The Chronic Venous Insufficiency Questionnaire (CVIQ) is also identified as a key contributor, influencing both the CFS PHY-Pre and CFS-Pre parameters, further emphasizing the complex interplay between chronic venous insufficiency and fatigue symptoms. Moreover, the analysis identifies other highly influential input parameters, such as the number of standing and sitting hours, the number of working days, CALF-CIR (calf circumference), and HCY (homocysteine levels), which all play significant roles in determining the outcomes. Conversely, the PR (pulse rate) parameter is highlighted as having one of the least impacts on the output, suggesting its relatively minor role in the context of this study. This comprehensive understanding of variable interrelationships provides valuable insights for targeting specific areas in future research and potential interventions.

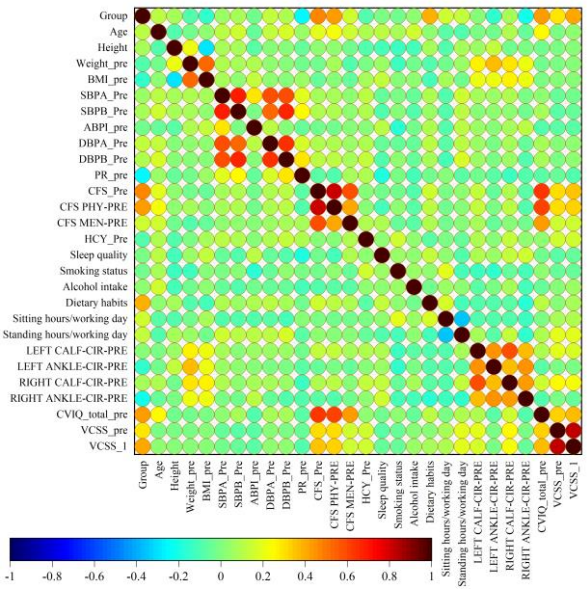

Fig. 1. Correlation matrix to examine how input and output variables are related to one another Evaluation of Model Suitability.

In the realm of classification challenges, Accuracy emerges as a frequently employed metric for evaluating overall model performance, taking into account True Positives (TP), True Negatives (TN), False Positives (FP), and False Negatives (FN). Despite its widespread use, Accuracy faces limitations in scenarios with imbalanced data, as it tends to favor the majority class, providing limited insights. The mathematical expression for Accuracy is defined in Eq. (20):

$$Accuracy = \frac{TP + TN}{TP + TN + FP + FN} \tag{20}$$

To overcome this restriction, three more measures are used: $F1 - Score, Precision$, and $Recall$. To reduce False Negatives, recall measures a model's capacity to accurately identify every pertinent instance inside a given class. By quantifying the precision of positive predictions, False Positives are decreased. Combining Precision and Recall, the F1-Score offers a balanced evaluation that is particularly helpful in situations when the data is unbalanced. Together, these metrics which are represented by mathematical formulae (Eq. 21–23) help to provide a more complete picture of the efficacy of a categorization model.

$$Precision = \frac{TP}{TP + FP} \tag{21}$$

$$Recall = TPR = \frac{TP}{P} = \frac{TP}{TP + FN} \tag{21}$$

$$F1\_score = \frac{2 \times Recall \times Precision}{Recall + Precision} \tag{23}$$

V. Results

To improve the accuracy of classifying and predicting VCSS before and after one month of yoga exercises, this study utilized two optimization algorithms: Crystal Structure Algorithm (CSA) and Fire Hawk Optimizer (FHO). The data, involving 100 patients, underwent careful evaluation in both training and testing phases following the implementation of these algorithms. The main objective is to refine and optimize model parameters using the mentioned algorithms.

Fig. 2 shows the convergence of developed hybrid models. VCSS-Pre, the GPCS, and GPFH models commenced iterations with nearly identical Precision. Eventually, the GPCS model achieved optimal accuracy in 100 iterations (with 0.860 value), while the GPFH model took 110 iterations (in 0.870). In contrast, in VCSS-1, the GPFH model started with lower accuracy than GPCS, reaching higher accuracy in the 80th iteration (in 0.910 accuracy value), while GPCS reached convergence in the 120th iteration (with 0.900).

Table I showcases extensive metrics, encompassing $Accuracy, Precision, Recall,$ and $F1\ Score$, across all models for the training and test phases. Notably, the GPFH model exhibits excellent performance in both VCSS-Pre and VCSS-1. Specifically, for VCSS-Pre, the model achieves a Precision of 0.870, Accuracy of 0.877, Recall of 0.870, and F1-score of 0.872. Similarly, in the case of VCSS-1, the GPFH model attains $Accuracy, Recall$, and $F1 - score$ values of 0.910, along with a Precision value of 0.916. Fig. 3 presents a bar plot that visually assesses the performance of the advanced models. Furthermore, it provides additional insights into the achieved results. For instance, it is observable that the GPFH, GPCS, and GPC models showcase optimal performance.

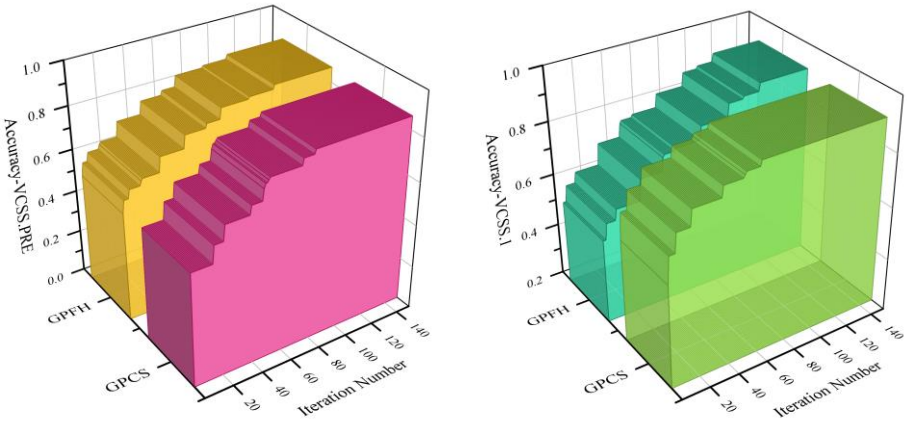

Fig. 2. Convergence curve of hybrid models.

TABLE I. RESULT OF PRESENTED MODELS

	Model	Part	Metric value			
			Accuracy	***Precision***	***Recall***	***F1 _Score***
VCSS – PRE	***GPC***	*Train*	0.900	0.913	0.900	0.901
		Test	0.733	0.759	0.733	0.737
		All	0.850	0.868	0.850	0.853
	GPFH	*Train*	0.929	0.937	0.929	0.930
		Test	0.733	0.739	0.733	0.735
		All	0.870	0.877	0.870	0.872
	GPCS	*Train*	0.900	0.915	0.900	0.900
		Test	0.767	0.771	0.767	0.767
		All	0.860	0.871	0.860	0.861
VCSS – 1	***GPC***	*Train*	0.957	0.958	0.957	0.957
		Test	0.733	0.733	0.733	0.733
		All	0.890	0.890	0.890	0.890
	GPFH	*Train*	0.957	0.969	0.957	0.959
		Test	0.800	0.800	0.800	0.798
		All	0.910	0.916	0.910	0.910
	GPCS	*Train*	0.914	0.926	0.914	0.917
		Test	0.867	0.871	0.867	0.867
		All	0.900	0.903	0.900	0.901

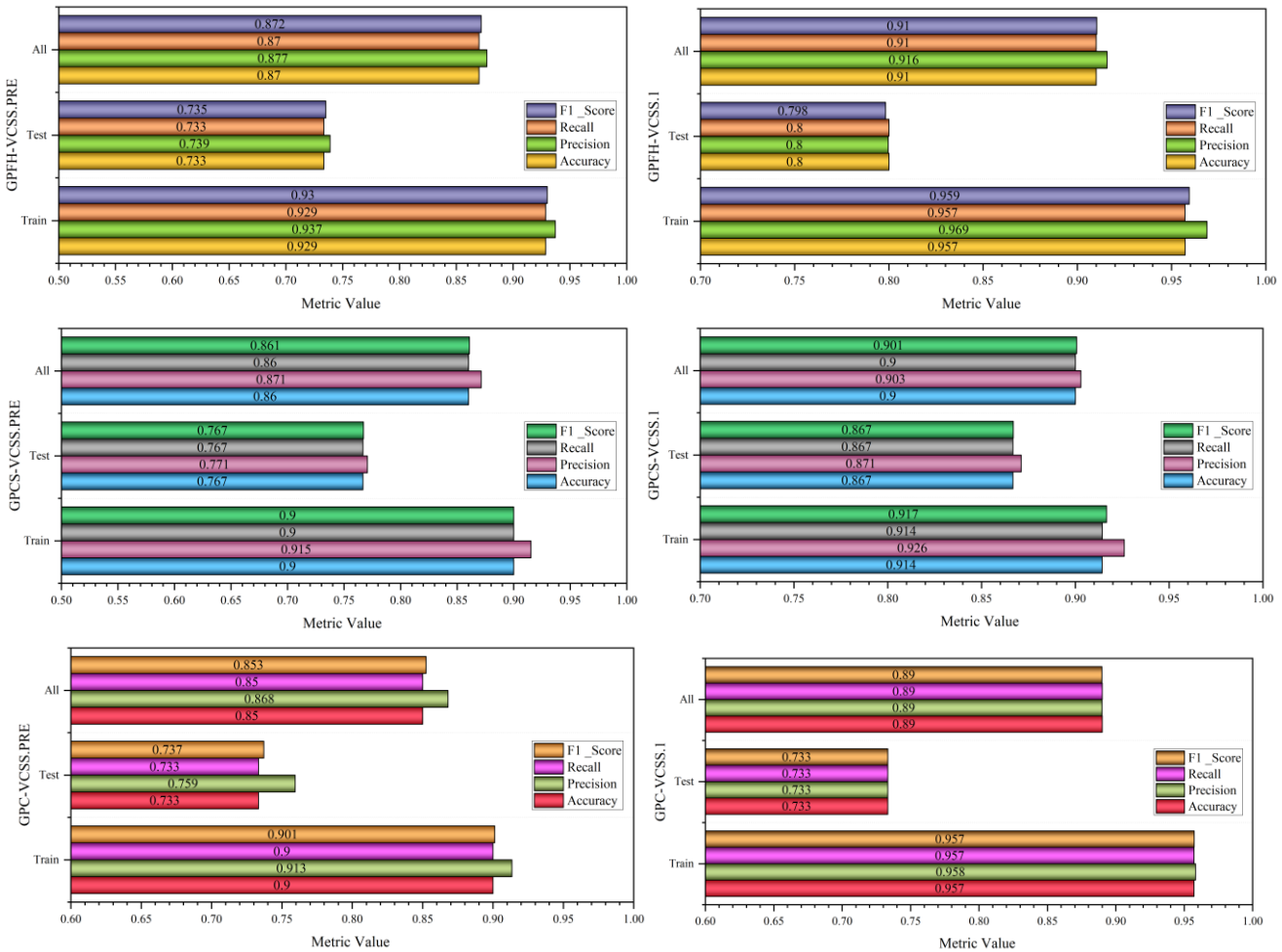

Fig. 3. Bar plot to visually evaluate the created models' performance.

Based on VCSS scores, patients are classified into four groups: Absent (0-5), Mild (6-10), Moderate (11-20), and Severe (21-30) condition. Concerning Precision in VCSS-Pre, as presented in Table II, the GPFH and GPCS models exhibit similar and close performance. Notably, for the Severe condition, both models achieved a value of 1. The GPFH model demonstrates superior performance for Mild and Moderate conditions with values of 0.841 and 0.950, respectively. However, for the Absent condition, the GPCS model outperforms with a value of 0.733. In Table III, considering the Precision values for VCSS-1, both the GPFH and GPCS models exhibit identical values for Severe conditions at 1. However, for Mild (0.912) and Moderate conditions (0.957), the GPFH model outperforms. Notably, akin to VCSS-Pre, in Absent conditions, the GPCS model demonstrates superior performance with a value of 0.813.

TABLE II. PERFORMANCE EVALUATION INDICES FOR THE DEVELOPED MODELS FOR VCSS-PRE

Model	*Condition*	*Metric value*		
		Precision	*Recall*	*F1 − score*
GPC	*Absent*	0.688	0.917	0.786
	Mild	0.804	0.881	0.841
	Moderate	0.972	0.796	0.875
	Severe	1.000	1.000	1.000
GPFH	*Absent*	0.714	0.833	0.769
	Mild	0.841	0.881	0.861
	Moderate	0.950	0.864	0.905
	Severe	1.000	1.000	1.000
GPCS	*Absent*	0.733	0.917	0.815
	Mild	0.826	0.905	0.864
	Moderate	0.946	0.796	0.864
	Severe	1.000	1.000	1.000

TABLE III. PERFORMANCE EVALUATION INDICES FOR THE DEVELOPED MODELS FOR VCSS-1

Model	*Condition*	*Metric value*		
		Precision	*Recall*	*F1 − score*
GPC	*Absent*	0.867	0.929	0.897
	Mild	0.861	0.838	0.849
	Moderate	0.915	0.915	0.915
	Severe	1.000	1.000	1.000
GPFH	*Absent*	0.778	1.000	0.875
	Mild	0.912	0.838	0.873
	Moderate	0.957	0.936	0.946
	Severe	1.000	1.000	1.000
GPCS	*Absent*	0.813	0.929	0.867
	Mild	0.865	0.865	0.865
	Moderate	0.956	0.915	0.935
	Severe	1.000	0.100	1.000

Fig. 4 shows a 3D drop line plot illustrating the difference between measured and forecast values for $VCSS - Pre$ and $VCSS - 1$. Separate graphs are included for each category ($Absent, Mild, Moderate$, and $Severe$), which comprehensively assesses the models' efficacy in classifying.

Upon reviewing the VCSS-Pre diagram, it becomes evident that 12 individuals fall under the Absent category, 42 in Mild, 44 in Moderate, and 2 in Severe. Significantly, the GPC and GPCS models stand out for their remarkable accuracy in classifying the Absent section. In this section, the models demonstrate exceptional Precision in predictions, with a one-unit difference, highlighting the capability to categorize individuals accurately. In Mild and Moderate conditions, the GPCS and GPFH models showcase superior performance with subtle distinctions. In the Severe section, three models demonstrate identical performance.

As illustrated in the figure for VCSS-1, the recorded counts for patients in the $Absent, Mild, Moderate,$ and $Severe$ categories are 14, 37, 47, and 2, individually. Notably, the GPFH model exhibits superior performance in the Absent and Moderate conditions, particularly in the Absent category, where it achieves error-free predictions. The GPCS model performs best in Mild conditions, and for Severe conditions, all utilized models demonstrate superior performance.

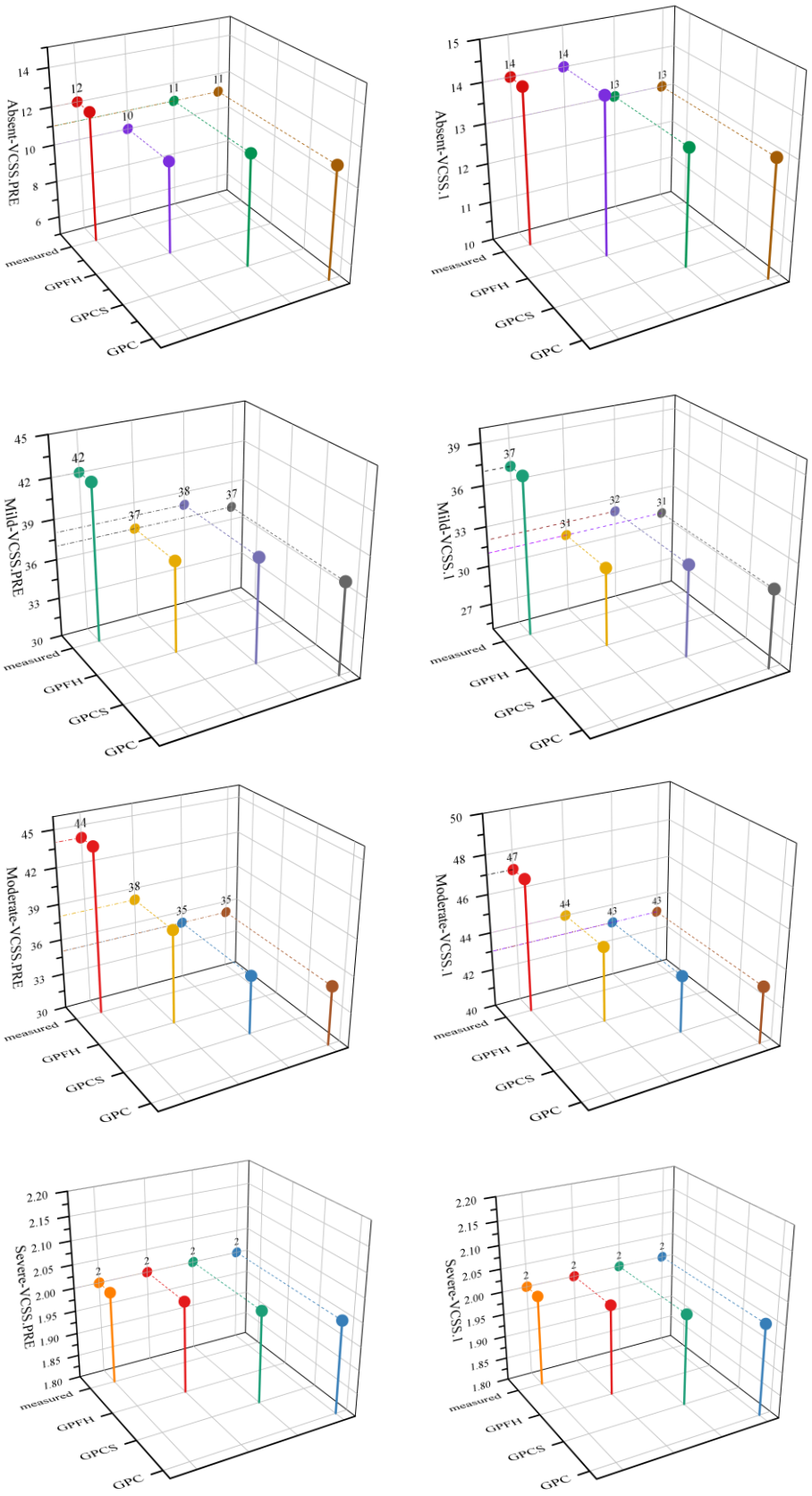

Fig. 4. 3D drop line plot for the difference between measured and forecast values.

Fig. 5 shows the confusion matrix. A confusion matrix summarizes the predictions of the ML model, offering a detailed assessment of its performance in terms of $Accuracy, Precision, Recall,$ and $F1-score$ measures for evaluating effectiveness. Table III displays the confusion matrix corresponding to VCSS-Pre and VCSS-1. In VCSS-Pre, the GPFH model correctly classified 87 patients, breaking down into 10 Absent, 37 Mild, 38 Moderate, and 2 Severe conditions, while 13 patients were misclassified. The GPCS model takes the second position, with 86 patients correctly classified and 14 misclassified. The GPC model ranks third, with 15 patients misclassified; in the context of VCSS-1, the GPFH model successfully classified 91 patients (14 in Absent, 31 in Mild, 44 in Moderate, and 2 in Severe conditions) with only nine misclassifications. The GPCS model secured 90 accurate predictions and 10 incorrect ones, while the GPC model claimed the third rank with 89 correct predictions and 11 incorrect ones.

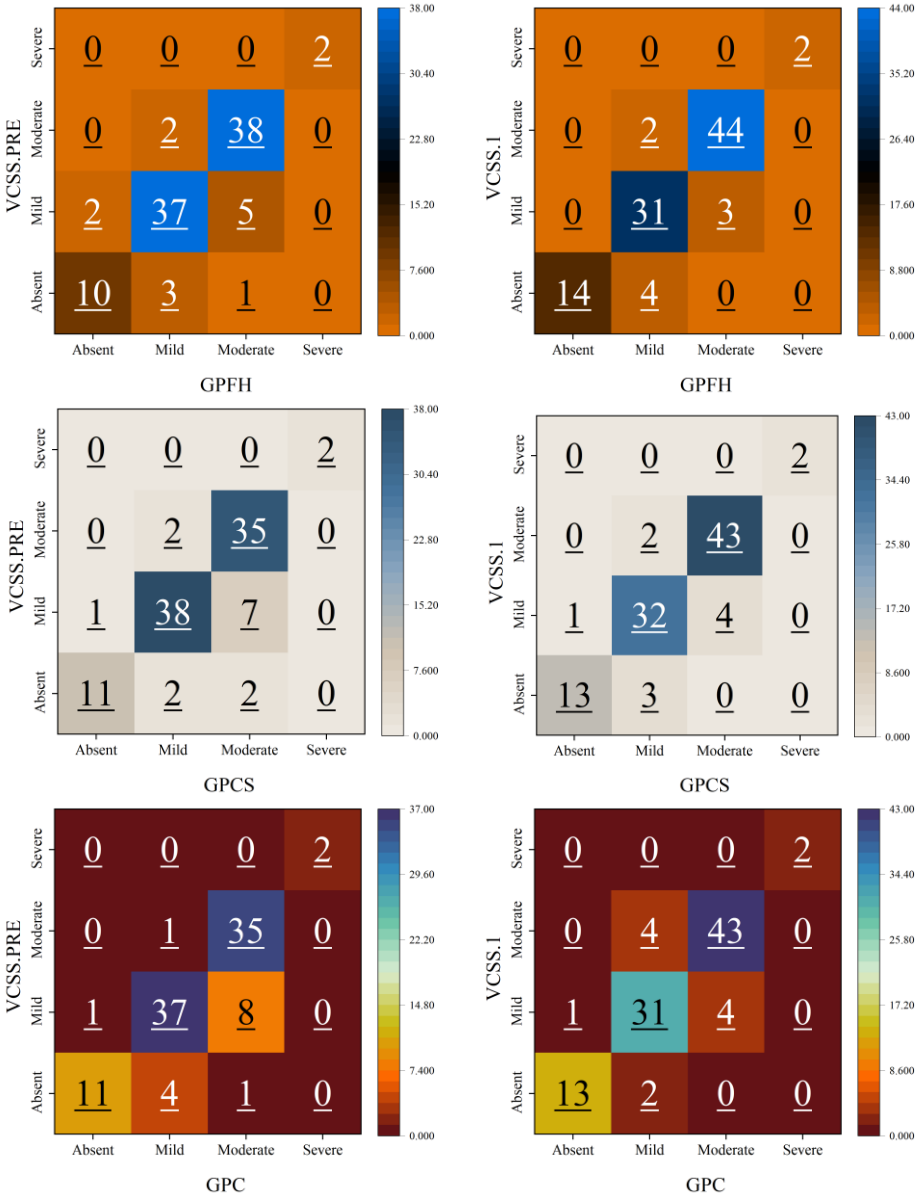

Fig. 5. Confusion matrix for each model's accuracy.

The Receiver Operating Characteristic (ROC) is a visual tool employed in classification to assess a model's performance by mapping the interplay between its false positive rate and true positive rate across diverse thresholds. Illustrating the discriminative capacity of a model, the ROC curve provides a comprehensive overview of its ability to distinguish between classes. Based on the top-performing GPFH model in Fig. 6, the ROC curve analysis indicates that this model serves as a classifier with acceptable performance in predicting VCSS-Pre for Moderate conditions. Within the VCSS-1 framework, the GPC model demonstrates superior performance for Absent and Mild conditions, with curves approaching 1 for each. Finally, it is noteworthy that the Micro Average, drawn for both VCSS-Pre and VCSS-1, supports the best performance in VCSS-1. Consequently, it can be inferred that one month of yoga practice affects CVI.

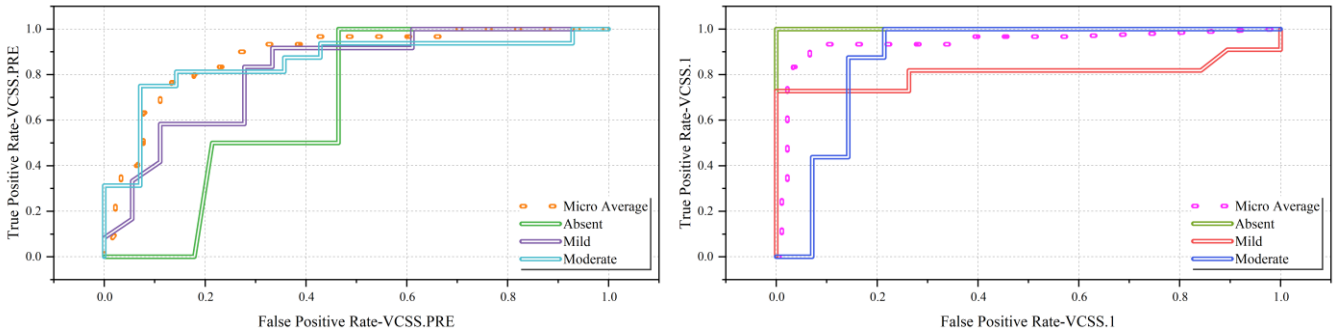

Fig. 6. The outcome is derived from the ROC curve.

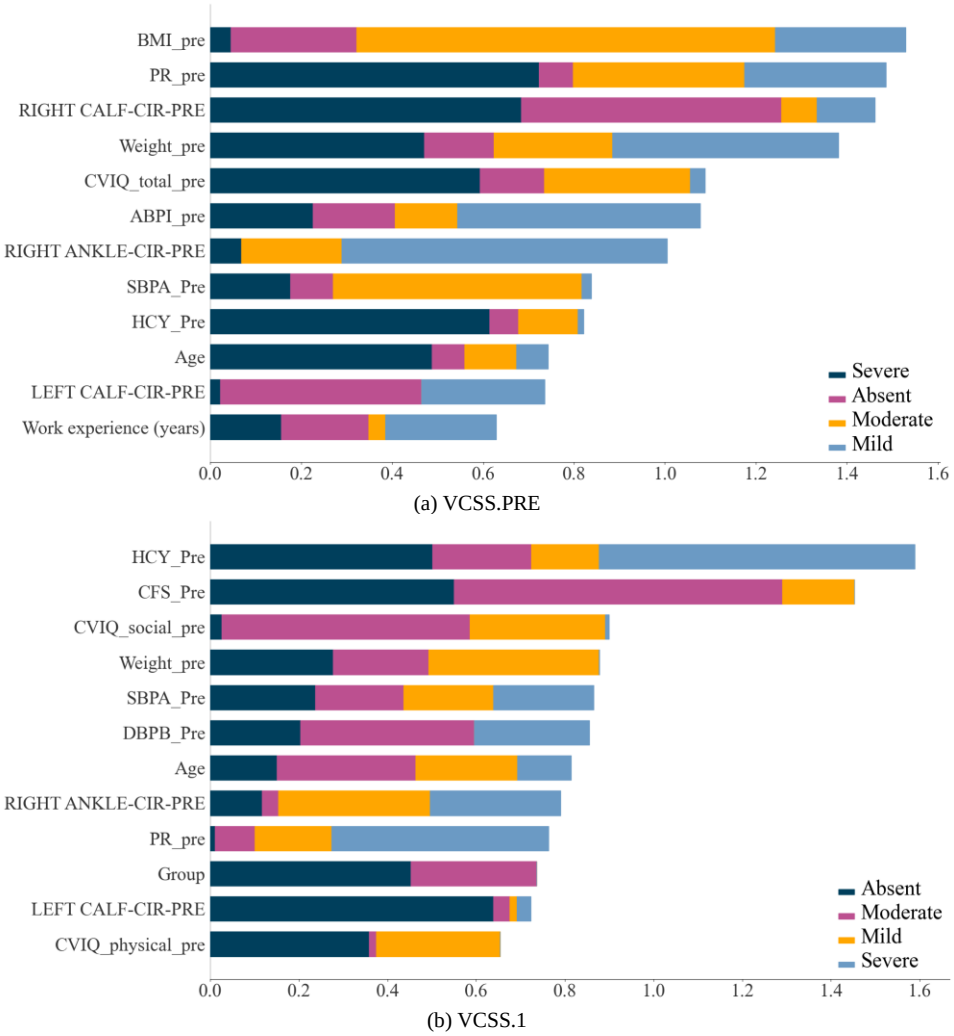

(a) VCSS.PRE

(b) VCSS.1

Fig. 7. Impact of input features on model outputs based on SHAP values.

Fig. 7, visually represents the impact of input features on model outputs for predicting symptoms related to CVI based on SHAP (Shapley Additive exPlanations) values. SHAP values are used to interpret the output of machine learning models, providing insights into how much each feature contributes to the prediction. The figure is divided into two plots: (a) VCSS.PRE and (b) VCSS.1, each showing the influence of various input features on the VCSS-Pre and VCSS-1 outcomes, respectively. The VCSS-Pre captures the symptoms observed before the initiation of yoga practices, while VCSS-1 reflects the symptoms after one month of participating in yoga sessions. In plot (a), the features are ranked by their influence on the VCSS-Pre output, with BMI_pre (Body Mass Index before yoga) and PR_pre (Pulse Rate before yoga) showing significant impacts across all severity levels—Severe, Absent, Moderate, and Mild. The RIGHT CALF-CIR-PRE (right calf circumference before yoga) and other physical indicators like the ABPI_pre (Ankle-Brachial Pressure Index before yoga) also contribute

substantially to the prediction outcomes. Plot (b) of the figure highlights the impact of input features on the VCSS-1 outcome. Notably, HCY_Pre (Homocysteine levels before yoga) and CFS_Pre (Chronic Fatigue Syndrome before yoga) emerge as the most influential features, particularly in the Severe category. Other factors, such as CVIQ_social_pre (Chronic Venous Insufficiency Questionnaire-social before yoga) and SBPA_Pre (Systolic Blood Pressure Type A before yoga), also show notable contributions to the model's predictions post-yoga intervention. The colored bars represent different severity levels, with each feature influencing these categories to varying degrees. This detailed analysis helps identify which features are most critical in predicting varicose vein symptoms and how these influences change after yoga intervention. The visual breakdown provides a clear understanding of how input variables contribute to the model's outputs, offering valuable insights for future research and potential therapeutic strategies in managing CVI.

VI. Conclusion

Chronic Venous Insufficiency (CVI) is characterized by impaired blood flow to the heart due to damaged or weakened valves in the leg veins, resulting in symptoms such as swelling, pain, skin alterations, and, more severe instances, persistent ulcers. This article aims to assess the impact of yoga exercises on alleviating symptoms in individuals with CVI. Employing a machine learning technique, the study predicts and categorizes symptoms before and one month after participating in yoga exercises. To ensure optimal performance, the selected model, Gaussian Process Classifier (GPC), for this study went through final optimization utilizing two optimizers, namely the Crystal Structure Algorithm (CSA) and the Fire Hawk Optimizer (FHO). A comprehensive evaluation was performed on 100 patients diagnosed with CVI. This assessment employed key criteria, including $Accuracy, Precision, Recall$, and $F1-score$. The resulting outcomes are presented as follows. In VCSS-Pre, concerning the F1-Score criterion, the GPFH model outperforms the GPCS and GPC models by 1.26% and 2.18%, respectively. Additionally, this superiority in Recall quality translates to 1.15% and 2.3%, respectively. Moreover, In the prediction of VCSS_1, the GPFH model demonstrates superior performance in F1_Score and Recall criteria compared to the GPCS (1% and 1.1%, respectively) and GPC (2.2% for both criteria) models.

Future studies on CVI and its management through yoga and machine learning-driven prediction models could explore several promising avenues. First, expanding the study to include a larger and more diverse patient cohort would enhance the generalizability of the findings, allowing for a more comprehensive understanding of the effectiveness of yoga in various demographic groups and across different stages of CVI. Additionally, longitudinal studies tracking patients over an extended period could provide valuable insights into the long-term effects of yoga on CVI symptoms, as well as any potential cumulative benefits. Another important area for future research is the integration of other complementary therapies with yoga, such as dietary modifications, physical therapy, or mindfulness practices. Investigating the combined impact of these approaches could lead to a more holistic treatment framework, addressing not only the physical but also the psychological aspects of CVI. On the machine learning front, future studies could explore the application of more advanced models, such as deep learning or ensemble methods, to enhance prediction accuracy and robustness. Additionally, incorporating real-time monitoring and data collection through wearable devices could provide more granular data, enabling more precise symptom tracking and personalized intervention strategies.

References

[1] T. S. Church et al., “Trends over 5 decades in US occupation-related physical activity and their associations with obesity,” PLoS One, vol. 6, no. 5, p. e19657, 2011.

[2] S. R. Patel et al., “Real-world experiences with yoga on cancer-related symptoms in women with breast cancer,” Glob Adv Health Med, vol. 10, p. 2164956120984140, 2021.

[3] J. Bames et al., “Standardized use of the terms" sedentary" and" sedentary behaviours",” Applied Physiology Nutrition and Metabolism-Physiologie Appliquee Nutrition Et Metabolisme, vol. 37, pp. 540–542, 2012.

[4] M. T. Hamilton, D. G. Hamilton, and T. W. Zderic, “Sedentary behavior as a mediator of type 2 diabetes,” Diabetes and Physical Activity, vol. 60, pp. 11–26, 2014.

[5] F. Q. S. Dzakpasu et al., “Musculoskeletal pain and sedentary behaviour in occupational and non-occupational settings: a systematic review with meta-analysis,” International Journal of Behavioral Nutrition and Physical Activity, vol. 18, no. 1, pp. 1–56, 2021.

[6] D. Shen et al., “Sedentary behavior and incident cancer: a meta-analysis of prospective studies,” PLoS One, vol. 9, no. 8, p. e105709, 2014.

[7] S. C. Gilchrist et al., “Association of sedentary behavior with cancer mortality in middle-aged and older US adults,” JAMA Oncol, vol. 6, no. 8, pp. 1210–1217, 2020.

[8] S. Carter, Y. Hartman, S. Holder, D. H. Thijssen, and N. D. Hopkins, “Sedentary Behavior and Cardiovascular Disease Risk: Mediating Mechanisms,” Exerc Sport Sci Rev, vol. 45, no. 2, 2017.

[9] A. K. Chomistek et al., “Relationship of sedentary behavior and physical activity to incident cardiovascular disease: results from the Women’s Health Initiative,” J Am Coll Cardiol, vol. 61, no. 23, pp. 2346–2354, 2013.

[10] N. M. Hamburg, “The legs are a pathway to the heart: connections between chronic venous insufficiency and cardiovascular disease,” Eur Heart J, vol. 42, no. 40, pp. 4166–4168, Oct. 2021, doi: 10.1093/eurheartj/ehab589.

[11] J. D. Raffetto and R. A. Khalil, “Mechanisms of lower extremity vein dysfunction in chronic venous disease and implications in management of varicose veins,” Vessel Plus, vol. 5, 2021.

[12] A. Thibert, N. Briche, B. D. Vernizeau, F. Mougin-Guillaume, and S. Béliard, “Systematic review of adapted physical activity and therapeutic education of patients with chronic venous disease,” J Vasc Surg Venous Lymphat Disord, 2022.

[13] H. D. Vlajinac, Đ. J. Radak, J. M. Marinković, and M. Ž. Maksimović, “Risk factors for chronic venous disease,” Phlebology, vol. 27, no. 8, pp. 416–422, 2012.

[14] E. Halliwell, K. Dawson, and S. Burkey, “A randomized experimental evaluation of a yoga-based body image intervention,” Body Image, vol. 28, pp. 119–127, 2019.

[15] M. Anusha, S. Dubey, P. S. Raju, and I. A. Pasha, “Real–time yoga activity with assistance of embedded based smart yoga mat,” in 2019 2nd International Conference on Innovations in Electronics, Signal Processing and Communication (IESC), IEEE, 2019, pp. 1–6.

[16] T. Field, “Yoga research review,” Complement Ther Clin Pract, vol. 24, pp. 145–161, 2016.

[17] D. Neumark-Sztainer, A. W. Watts, and S. Rydell, “Yoga and body image: How do young adults practicing yoga describe its impact on their body image?,” Body Image, vol. 27, pp. 156–168, 2018.

[18] D. Kumar and A. Sinha, Yoga pose detection and classification using deep learning. LAP LAMBERT Academic Publishing London, 2020.

[19] T. Y. Park et al., "Epidemiological trend of pulmonary thromboembolism at a tertiary hospital in Korea," Korean J Intern Med, vol. 32, no. 6, p. 1037, 2017.

[20] D. Morrone and V. Morrone, "Acute pulmonary embolism: focus on the clinical picture," Korean Circ J, vol. 48, no. 5, pp. 365–381, 2018.

[21] A. Pizano et al., "Association between cardiac conditions with venous leg ulcers in patients with chronic venous insufficiency," Phlebology, vol. 38, no. 4, pp. 281–286, 2023.

[22] W. A. Marston et al., "Economic benefit of a novel dual-mode ambulatory compression device for treatment of chronic venous leg ulcers in a randomized clinical trial," J Vasc Surg Venous Lymphat Disord, vol. 8, no. 6, pp. 1031–1040, 2020.

[23] Y. Kim, C. Y. M. Png, B. J. Sumpio, C. S. DeCarlo, and A. Dua, "Defining the human and health care costs of chronic venous insufficiency," in Seminars in Vascular Surgery, Elsevier, 2021, pp. 59–64.

[24] N. Maddukuri and S. R. Ummity, "Yoga Pose prediction using Transfer Learning Based Neural Networks," 2023.

[25] J. Azar, A. Rao, and A. Oropallo, "Chronic venous insufficiency: a comprehensive review of management," J Wound Care, vol. 31, no. 6, pp. 510–519, 2022.

[26] I. Sudoł-Szopińska, A. Bogdan, T. Szopiński, A. K. Panorska, and M. Kołodziejczak, "Prevalence of chronic venous disorders among employees working in prolonged sitting and standing postures," International journal of occupational safety and ergonomics, vol. 17, no. 2, pp. 165–173, 2011.

[27] M. A. Passman et al., "Validation of venous clinical severity score (VCSS) with other venous severity assessment tools from the American venous forum, national venous screening program," J Vasc Surg, vol. 54, no. 6, pp. 2S-9S, 2011.

[28] R. Zulpe, "An Experimental study of yoga therapy on varicose vein," 2023.

[29] M. A. Chaoul and L. Cohen, "Rethinking yoga and the application of yoga in modern medicine," Crosscurrents, vol. 60, no. 2, pp. 144–167, 2010.

[30] T. Field, "Yoga research review," Complement Ther Clin Pract, vol. 24, pp. 145–161, 2016.

[31] M. Kuss, C. E. Rasmussen, and R. Herbrich, "Assessing Approximate Inference for Binary Gaussian Process Classification.," Journal of machine learning research, vol. 6, no. 10, 2005.

[32] M. Azizi, S. Talatahari, and A. H. Gandomi, "Fire Hawk Optimizer: A novel metaheuristic algorithm," Artif Intell Rev, vol. 56, no. 1, pp. 287–363, 2023.

[33] B. A. Averill and P. Eldredge, "Chemistry: principles, patterns, and applications," (No Title), 2007.

[34] S. Talatahari, M. Azizi, M. Tolouei, B. Talatahari, and P. Sareh, "Crystal structure algorithm (CryStAl): a metaheuristic optimization method," IEEE Access, vol. 9, pp. 71244–71261, 2021.

[35] C. Pete et al., "Crisp-Dm 1.0—Step-by-step data mining guide," Cris. Consort, p. 76, 2000.

[36] M. Botlagunta et al., "Classification and diagnostic prediction of breast cancer metastasis on clinical data using machine learning algorithms," Sci Rep, vol. 13, no. 1, p. 485, 2023.

[37] L. Torgo, Data mining with R: learning with case studies. chapman and hall/CRC, 2011.